Multiresolution Upscaling of Multiscale Heterogeneous Oil Reservoirs Using Wavelet Transformations

Siroos Azizmohammadi[i], Bahram Dabir[ii], Muhammad Sahimi[iii]

ABSTRACT

A general multiresolution approach is developed and applied to upscaling of multiscale 2D heterogeneous reservoirs. The method uses the wavelet transformations to the original detailed description of the reservoir, with finer resolution introduced in region of potentially high flow rate (high permeability) and coarser, homogenized property descriptions applied throughout the bulk of the model. Wavelet transformations are currently recognized as the most efficient method of data compression. The method is applied to flow problem (steady single-phase flow) and transport problem (miscible displacement process). In this way, pressure is computed on the coarse-grid using upscaled properties. These pressures are then used to compute the pressure at the small scale within each coarse block. Thus, an approximation for the pressure is obtained without ever having to solve the full fine-grid problem, saving CPU time and memory. Finally, velocity field, the most important key component of fluid flow process, is calculated using obtained pressure field. The results of two problems show good agreement with full fine-grid solution.

KEYWORDS

Upscaling, Wavelet Transform, Heterogeneous Oil Reservoir, Miscible Displacement, Single-Phase Flow, Particle Tracking Method, Random Walk Method.

1. INTRODUCTION

The data describing the basic geophysical properties of a reservoir are important input to any method for simulating the production of hydrocarbons. These data, usually generated by geostatistical methods, are often given on a very fine-scale. These fine-scale models routinely contain 10^6 to 10^8 grid blocks. These models often cannot be used directly in a reservoir simulation because of the time and memory required for solving the pressure field on the fine-grid. Thus, the data have to be upscaled to a coarser representation before they are used in a simulator. Upscaling methods try to reduce the size of the geological model without losing accuracy (the basic idea of data compression). On the other hand, upscaling is a technique that transforms a detailed geological model to a coarse-grid simulation model so that the fluid flow behaviors in the two systems are the same. Accurate upscaling consists of two inseparable parts: gridding and averaging. The former intends to capture the global geological features of a geological model, and the latter focuses on preserving the local geological details within a coarse-grid block. Upscaling is necessary because available computers are usually memory-limited and are not fast enough to simulate the detailed geological models derived from reservoir characterization. Even as computers increase in memory size and speed, accurate upscaling will always be a more cost-efficient method for simulating large, complicated reservoirs.

Averaging, one of the key components of upscaling, calculates the effective properties for a coarse simulation grid that preserves fine-grid fluid flow dynamics (including pressure and flow rate) within the coarse-grid block. Averaging methods range from the simple averages (arithmetic, harmonic and geometric means) to numerical simulation methods (pressure solver). Intermediate methods are, for example, power-law averaging and renormalization. Simple and intermediate methods are fast but less accurate, while numerical simulations are accurate but time-consuming. A fast and accurate averaging method is demanded for upscaling of very large geological models.

The averaging problem is an old, unsolved problem of petroleum reservoir engineering. It is well known that the effective permeabilities for a layered, permeable medium with no cross flow are the arithmetic mean for flows parallel to the layering direction and the harmonic mean for flows perpendicular to the layering direction [23].

[i] Siroos Azizmohammadi, PhD in Chemical Engineering (e-mail: s_azizmohammadi@yahoo.com).
[ii] Bahram Dabir, Professor of Chemical Engineering, Amirkabir University of Technology, Tehran, Iran (e-mail: drbdabir@aut.ac.ir).
[iii] Muhammad Sahimi, Professor of Chemical Engineering, University of Southern California (USC), LosAngeles, USA, (e-mail: moe@usc.edu).

Cardwell and Parsons [1] proved that when fluid flow crosses over layers in a permeable medium, the arithmetic mean and harmonic mean give only the upper and lower limits, respectively, for the effective permeability of a heterogeneous permeable medium, rather than the effective permeabilities themselves. They concluded that the effective permeability of a heterogeneous permeable medium lies between the arithmetic and harmonic limits. Warren and Price [2] conducted several numerical experiments to investigate the effective permeability of a heterogeneous permeable medium and concluded that the effective permeability of the randomly generated 3D permeable medium equals the geometric mean of the individual permeabilities. Because of the technical limitations at that time, their conclusion actually is good only for purely uncorrelated permeability fields, which seldom exists in real petroleum reservoirs.

The most accurate way of calculating the effective permeability of a large, coarse-grid block containing many fine-grid blocks is by solving flow equations with constant-pressure and no-flow boundary conditions [2]-[3], [27] or with periodic boundary conditions [4], regardless of the extensive computation required. This approach is referred to as a pressure-solver technique by many researchers because it involves solving the fine-grid pressure distribution first and then calculating the effective permeability with the pressure drop and the calculated flux. Because of computing limitations, pressure-solver techniques may not be practical for extremely large geological models.

There are several averaging techniques intermediate between the traditional simple averaging methods and pressure-solver techniques. The most frequently used intermediate methods are renormalization [5]-[7] and power-law averaging [8], [9], [28]-[29]. Renormalization includes a series of multiple step calculations using an equivalent resistor network approach. The major drawback of the renormalization technique is the use of unrealistic boundary conditions, which may result in estimation errors over 100% [34]. However, some more current results [10] show that use of periodic boundary conditions may improve the accuracy of the renormalization method. Power-law averaging has been used extensively in research work on upscaling in recent years [5]-[7]. Power-law averaging is faster than the pressure-solver techniques, but it is not easy to use in practice because it requires empirical determination of the power-law averaging exponent through fine-grid simulation. The exponent can vary from one coarse-grid block to another. As a result, the use of a constant exponent for all coarse-grid blocks may result in large errors. The use of global upscaling [7] (focusing on global similarity between a geological model and its upscaled simulation model) drastically reduces the errors induced from averaging by minimizing heterogeneity in each coarse-grid block through a special gridding algorithm. One drawback for current global upscaling method is that the algorithm uses a power-law averaging method for averaging in each coarse-grid block. If the fine-grid permeabilities in each coarse-grid block were perfectly uncorrelated (white noise), the power-law method would be sufficiently accurate. Unfortunately, to make fine-grid permeabilities in all coarse-grid blocks perfectly uncorrelated is very difficult in practice. A comprehensive review of these upscaling methods can be found in the paper by Renard and de Marsily [11].

An alternative approach to upscaling is to solve pressure equation on the coarse-scale using upscaled properties while fine-scale information is introduced during the saturation update by using either a pressure or flux refinement [30], [31]. Guedes and Schiozer [32] used a similar approach and included gravity effects and well boundary conditions as source or sinks in one grid block. The refining technique developed in Hermitte and Guerillot [33] was used to obtain a continuous velocity field within each coarse-grid block. Arbogast and Bryant [34] developed an alternative approach in the context of a mixed finite element formulation. The pressure field was solved implicitly on a coarse mesh and Green functions were used to derive the fine-scale solution from the coarse-scale simulation. Hou et al. [14]-[15] developed a multiscale finite element method where finite element basis functions are calculated on a coarse mesh incorporating the fine-scale description of reservoir. These basis functions were then used to solve the elliptic problem on the coarse mesh for different types of boundary condition and to reconstruct the velocity field on the fine mesh.

A major objective of this study is to develop a fast and accurate averaging method that improves the traditional averaging methods for realistic reservoirs and substitute direct simulation methods for upscaling geological models. In this way, an automatic multiresolution upscaling technique based on wavelet transformations is presented in 2D heterogeneous reservoirs. A wavelet reconstruction method is used to provide for upsampling fine-scale property fields from information at various levels of coarser scale. The beauty of the method is that since the equivalent properties at different length scales are computed recursively, the interdependent influences of the heterogeneities on the scales are included effectively.

The outline of this paper is as follows. In section 2, we consider the historical and mathematical background of wavelet transform and its application to various flow processes upscaling in heterogeneous reservoirs. To ensure that the proposed method is accurate and practical, single-phase and miscible displacement simulations have been done as benchmarks to validate the method. Section 3 shows these results. Finally, discussion about the results and conclusion points has been presented in section 4.

2. THEORY

Wavelet transform, like the extensively used Fourier transform, is also kind of linear integral transforms. To understand the mechanism of the wavelet transform, one may begin with the familiar Fourier transform. Recall that for a given function $f(x)$ the corresponding Fourier transform takes the form [24]:

$$\hat{f}(\omega) = \int_{-\infty}^{+\infty} f(x)\, e^{-i\omega x} dx \qquad (1)$$

where ω is the angular frequency.

Although the above transform gives information about the content of a function in the frequency domain, it gives no information about the location of these frequencies in the spatial domain. Therefore, strictly speaking, a Fourier transform is applicable to a "homogeneous" system; otherwise, it only extracts "blend" properties. Figure 1 shows the schematic view of Fourier transform.

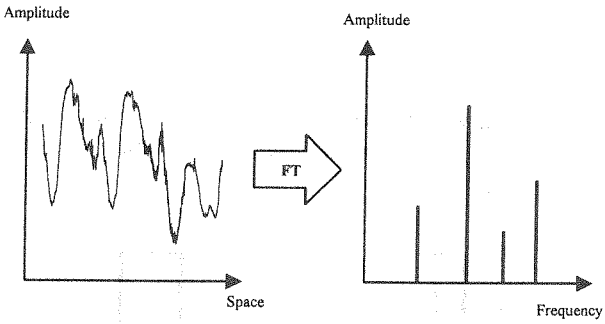

Figure 1- Fourier Transform (FT)

Spatially varying effects are quite common and are reminiscent of many natural and man-made phenomena, such as in seismic signals, non-stationary geophysical processes, and in reservoir rock property distributions. To extract information from such processes, a Fourier transform alone is, therefore, quite inadequate. This is because although Fourier transform gives the information of certain frequencies, this information cannot be effectively used, as it is not spatially localized. Ideally, one would have space and frequency information, simultaneously. One of the methods whish gives the space-frequency representation of a function (or process) but still remains within the Fourier transform framework is the windowed Fourier transform. By the windowed Fourier transform, spatial localization can be obtained by convoluting a windowing function $w(x)$ with the convolutional Fourier transform, as follows:

$$\hat{f}(\omega, s) = \int_{-\infty}^{+\infty} f(x)\, w(x-s)\, e^{-i\omega x} dx \qquad (2)$$

where s is the location of the center of the window. $\hat{f}(\omega, s)$ describes the spectral content of $f(x)$ around s within the window defined by $w(x)$.

Despite an ability to spatially localize information, the windowed Fourier transform suffers from several limitations. For example, because the spatial localization precision of the windowed Fourier transform is controlled by a scaling factor σ_w which is fixed for the windowed Fourier transform, if there are important local transient components of differing support size, then one cannot find a universally optimal $w(x)$ for effectively and precisely analyzing the process. Figure 2 shows the schematic view of windowed Fourier transform.

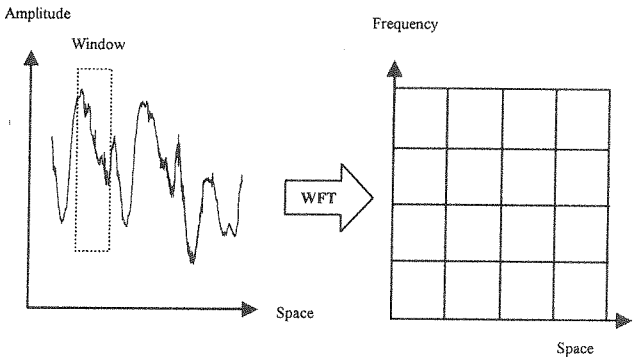

Figure 2- Windowed Fourier Transform (WFT)

The wavelet transform (Figure 3) was developed to address such limitations of the windowed Fourier transform and other similar transforms. It is windowed Fourier transform with variable window's size and is defined as a convolution of a given function $f(x)$ with a kernel function $\psi_{a,b}(x)$ as follows:

$$\hat{f}(a,b) = \int_{-\infty}^{+\infty} f(x)\, \psi_{a,b}(x)\, dx \qquad (3)$$

here a is a scale parameter, b is a translation parameter, and the family of functions $\psi_{a,b}(x)$ are called wavelet functions as:

$$\psi_{a,b}(x) = \frac{1}{\sqrt{a}} \psi\left(\frac{x-b}{a}\right) \qquad (4)$$

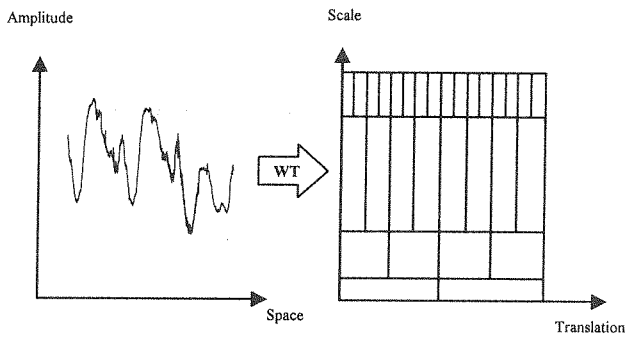

Figure 3a- Wavelet Transform (WT)

In contrast to the constant support length of the windowing function $w(x)$ in the windowed Fourier transform, the support length of wavelet functions $\psi_{a,b}(x)$ changes proportionally with the scale parameter a, i.e. increasing a will dilate and decreasing a will contract the wavelet function. In this way, in small scale, the wavelet function will have small support length; therefore wavelet transform will pick up higher frequency components and vice-versa. On the other hand, scale is similar to frequency and actually inverse of frequency and

translation is similar to spatial location.

Ideally, one would prefer both the support length and moving incremental step of the wavelet function to be small in small scale and vice versa. This can be easily accomplished by relating them to level of scale j or explicitly define:

$$a = a_0^j \tag{5}$$

and

$$b = kb_0a_0^j \tag{6}$$

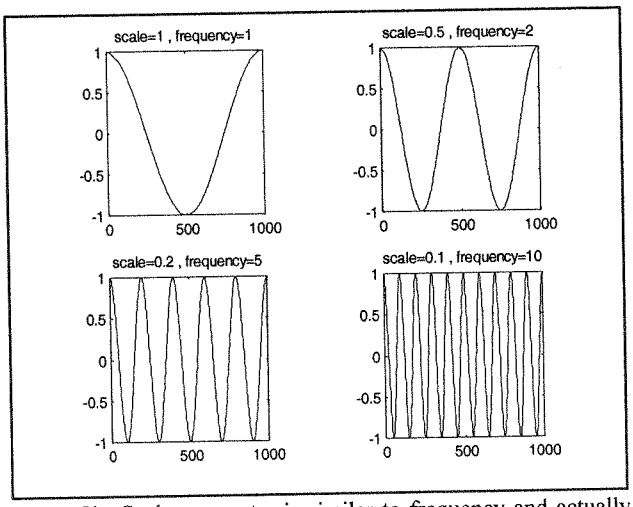

Figure 3b- Scale parameter is similar to frequency and actually inverse of frequency. Low frequencies (high scales) give global information of a signal, whereas high frequencies (low scales) yield detailed information of a signal.

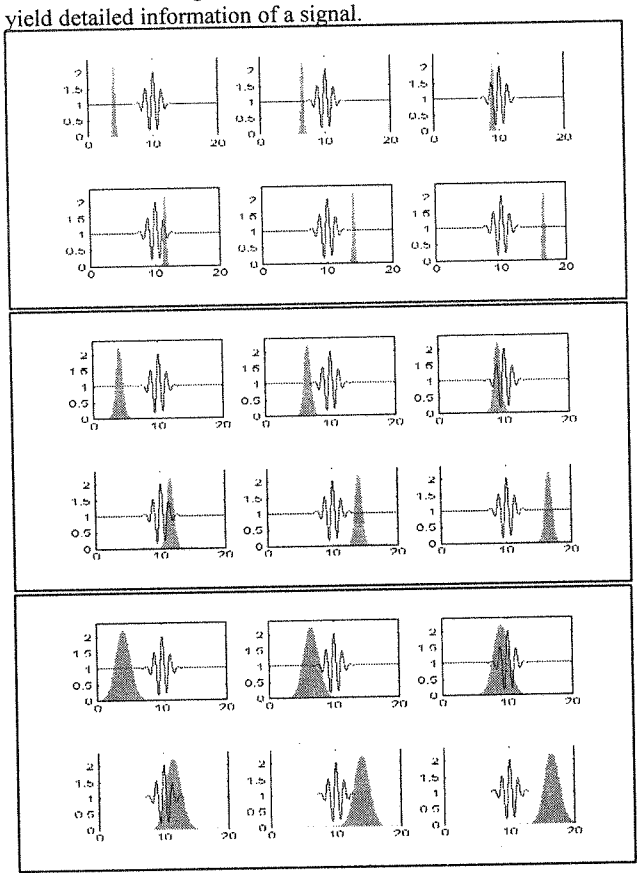

Figure 3c- Translation parameter is similar to space (top scale=1, middle scale=5, bottom scale=10).

where a_0 is a basic scale step size greater than 1, b_0 is the initial step size at scale 0, and k is an integer representing spatial index of data sequence. For the convenience of computation, one may assign, $a_0 = 2$ and normalize the initial system so that $b_0 = 1$.

A. Wavelet Functions and Coefficients

With the above convention, a family of wavelet functions can be written as:

$$\psi_{j,k}(x) = \frac{1}{\sqrt{2^j}}\psi\left(2^{-j}x - k\right) \tag{7}$$

$\psi(x)$ is '*wavelet function*' so-called mother wavelet. In addition to $\psi(x)$, there is other wavelet function $\phi(x)$ is called '*scaling function*' or father wavelet and so:

$$\phi_{j,k}(x) = \frac{1}{\sqrt{2^j}}\phi\left(2^{-j}x - k\right) \tag{8}$$

The Haar wavelets are the earliest and perhaps simplest known example of wavelet and scaling functions, which are presented in Figure 4.

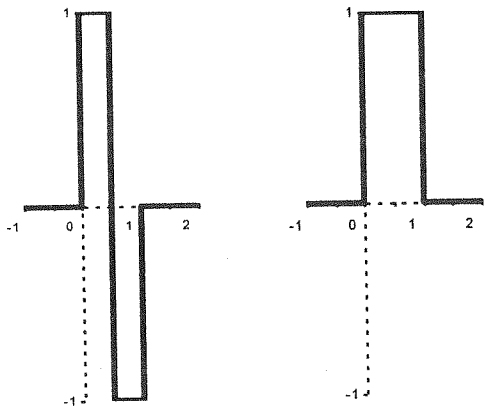

Figure 4- Haar wavelet (left) and scaling function (right)

Replacing Equations (7) and (8) in Equation (3) yields the '*detail*' and '*scale*' coefficients of transform, respectively. According to Mallat [16] the detail and scale coefficients in each level is related to scale coefficients of the finer level as:

$$D_{j,k} = \sum_l g_l S_{j-1,l+2k} \tag{9}$$

$$S_{j,k} = \sum_l h_l S_{j-1,l+2k} \tag{10}$$

g_l and h_l are the filter coefficients. For Haar wavelets $g_0 = -g_1 = 1/\sqrt{2}$ and $h_0 = h_1 = 1/\sqrt{2}$ while all other coefficients is zero[1]. The scale coefficients at the level $j = 0$ are taken to be the values of given function $f(x)$.

The above procedures for 1D data sequence can be extended to a 2D data as a tensor product of two 1D

wavelet functions. Based on this assumption, the scaling function for the 2D case is related to corresponding 1D scaling functions by:

$$\Phi_{j,k_1,k_2}(x,y) = \phi_{j,k_1}(x)\,\phi_{j,k_2}(y) \tag{11}$$

Also, there are three wavelet functions, which can be constructed using corresponding wavelet and scaling functions as follows:

$$\Psi^{(1)}_{j,k_1,k_2}(x,y) = \phi_{j,k_1}(x)\,\psi_{j,k_2}(y) \tag{12}$$

$$\Psi^{(2)}_{j,k_1,k_2}(x,y) = \psi_{j,k_1}(x)\,\phi_{j,k_2}(y) \tag{13}$$

$$\Psi^{(3)}_{j,k_1,k_2}(x,y) = \psi_{j,k_1}(x)\,\psi_{j,k_2}(y) \tag{14}$$

Then, one can obtain the scale and detail coefficients in 2D. First, a 1D Mallat algorithm [16] is applied in a given direction, e.g., the x-direction. One then applies the same 1D algorithm to the calculated coefficients in y-direction. Each application results in two coefficients and thus the four-wavelet coefficients (one scale and three detail coefficients) are obtained.

B. Wavelet Upscaling of Heterogeneous Reservoirs

It is well known that petroleum reservoirs are inherently heterogeneous and that flow performance of reservoirs is controlled by variability in reservoir properties at various scales. Therefore, to accurately describe reservoir performance, one needs to develop a method to first adequately reconstruct the fine-scale variability from sparsely distributed, coarser, multiscale samples, and then properly coarsen the fine-scale variability whenever necessary.

Suppose that the reservoir is represented by its permeability distribution, which is broad and correlated, and is obtained, either from extensive data (which is rare), or by limited field data and geostatistical methods. Figure 5 shows a typical 128×128 absolute permeability fine map (level $j = 0$) that was generated by a fractional Brownian motion (fBm) with Hurst exponent $H = 0.8$. It is assumed that the distribution has the finest possible structure, i.e., a more detailed map cannot be built because no information about permeability at finer length scale is available.

C. Algorithm

The procedure presented in the previous parts is used to upscale the absolute permeability distributions. Now we apply one-level wavelet transform to this permeability map using above procedure and obtain detail and scale coefficients of transform. Then we define two thresholds τ_S and τ_D, where τ_S is a measure of the permeability at a given block, and τ_D measures the contrast in permeability values between neighboring blocks. We then check the scale coefficient at each block. If it is higher than τ_S, then do nothing and move on to the next block. However, if it is smaller than τ_S, we check the detail coefficients and set to zero all of them that are smaller than τ_D. Setting detail coefficients to zero means that the neighbor of block is removed, i.e., the two blocks join and form a larger block.

Therefore, depending on the structure of the permeability map, a number of blocks in the original fine-scale model are coarsened. If permeability distribution is relatively narrow, the blocks are coarsened more or less uniformly throughout the model, whereas with a broad and correlated permeability distribution the coarsened blocks are scattered in the model. This algorithm is repeated again until no significant number of the blocks is coarsened (removed). Typically, after 3 or 4 levels the model can no longer be effectively coarsened, thus yielding very fast the final coarsened model for the fixed τ_S and τ_D. The level of the detail fixes the values of the thresholds that we would like to include in the model and the amount of computational time that we can afford. Preliminary investigations in 2D heterogeneous reservoirs model [17] indicate that, even with a broad permeability distribution and large values of τ_S and τ_D, the overall behavior of the fine-scale and the coarsened models are essentially identical.

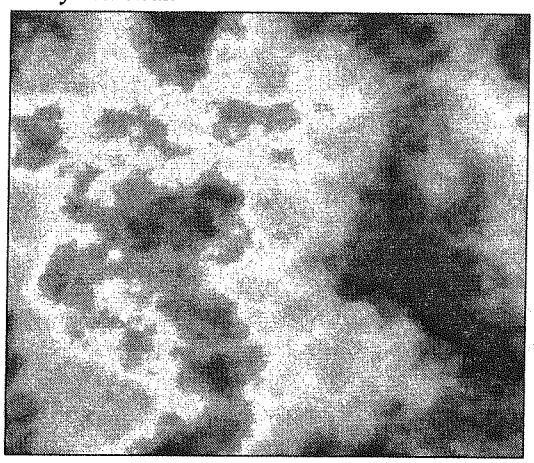

Figure 5- Fine permeability map fBm 128×128 with H=0.8

An important issue in upscaling is assignment of the effective permeabilities of the coarsened blocks. Once the size and shape of each coarsened block is determined, its effective permeability can be assigned by several methods. For example, one can assign the block permeability by carrying out single-phase flow calculations[18].

Alternatively, the permeabilities of the coarsened blocks can be assigned by calculating some sort of average permeability of the original fine-scale blocks that are contained within the coarsened blocks. Wavelet upscaling method carries out the coarsening process in such a way that the distribution of block permeabilities in the coarsened model automatically follows closely that of the original fine-scale model. Applying the inverse wavelet transform can do this step.

D. Flow Problem

As a flow problem, steady single-phase flow problem is

considered here. For steady incompressible flow, continuity equation (conservation of mass) is given by:

$$\nabla \cdot \mathbf{v} = 0 \tag{15}$$

Darcy's velocity law for fluid flow in porous media with neglecting gravity effects is[18]:

$$\mathbf{v} = -\frac{1}{\mu}\mathbf{k} \cdot \nabla p \tag{16}$$

where $\mathbf{v}$ is velocity vector, $\mathbf{k}$ the fine permeability tensor and p the pressure. Pressure equation arises by combining Equations (15) and (16) as follows:

$$\nabla.\left(\frac{1}{\mu}\mathbf{k} \cdot \nabla p\right) = 0 \tag{17}$$

The specific boundary conditions are Dirichlet type (constant pressure) in direction of flow and Neumann type (no-flow or impermeable) in perpendicular direction of flow. Numerical solution of Equation (17) with mentioned boundary conditions results fine pressure field.

For coarsened model pressure equation can be changed to:

$$\nabla \cdot \left(\frac{1}{\mu}\mathbf{k}_c \cdot \nabla p\right) = 0 \tag{18}$$

where $\mathbf{k}_c$ is the coarsened permeability tensor which is obtained by wavelet upscaling method presented in the previous part. The same boundary conditions as fine-scale can be used to solve coarse pressure field. Then fine pressure field can be computed from coarse pressure field by different ways.

E. Transport Problem

As a transport model, particle tracking method is used to simulate miscible displacement process. Particle tracking methods provide an efficient numerical algorithm for modeling large scale transport of solutes in heterogeneous porous media [20]. By contrast, continuum approaches involving finite difference or finite element solution methods generally suffer from numerical dispersion, primarily because of the large grid blocks required to model large scale systems. Furthermore, using particle tracking, plumes can be simulated at scales smaller than the grid block size, and source regions (zones in which particles are initially placed) can be smaller than the grid spacing. Particle tracking techniques have a long history of use in such applications (e.g., [19]-[21]). Application of random walk particle tracking method in solute transport (dispersion process), has been accepted by the hydrologic community. Here, to implement a model, a random walk particle tracking method was used to simulate transport problem.

The fundamental mass transport equation for transport of a nonreactive, dilute species in a saturated porous medium (with no sources or sinks) has the form [25]:

$$\frac{\partial C}{\partial t} + \nabla \cdot (\mathbf{v}C) - \nabla \cdot (\mathbf{D}\nabla C) = 0 \tag{19}$$

where C denotes the solute concentration in units of moles per liter, t is time, $\mathbf{v}$ designates the solute average pore-water velocity vector and $\mathbf{D}$ denotes the dispersion tensor. For an isotropic medium, the dispersion has the form[18]:

$$\mathbf{D} = (\alpha_T \mathrm{V} + D_0)\mathbf{I} + (\alpha_L - \alpha_T)\frac{\mathbf{vv}}{\mathrm{V}} \tag{20}$$

where α_L and α_T denote the longitudinal and transverse dispersivities, respectively, D_0 represents the molecular diffusion coefficient, $\mathrm{V} = |\mathbf{v}|$ is the magnitude of the velocity vector, $\mathbf{I}$ is the identity matrix and vv is the dyadic product of velocity vector.

Defining the two Cartesian coordinate axes as 1 and 2, the dispersion tensor given in Equation (20) can be written in matrix form as:

$$\mathbf{D} = \begin{bmatrix} \alpha_T \mathrm{V} + (\alpha_L - \alpha_T)\frac{v_1^2}{\mathrm{V}} + D_0 & (\alpha_L - \alpha_T)\frac{v_1 v_2}{\mathrm{V}} \\ (\alpha_L - \alpha_T)\frac{v_2 v_1}{\mathrm{V}} & \alpha_T \mathrm{V} + (\alpha_L - \alpha_T)\frac{v_2^2}{\mathrm{V}} + D_0 \end{bmatrix} \tag{21}$$

The general approach used in particle tracking is to replace the partial differential equation for the solute having concentration C, generally expressed by Equation (19), with random walk displacements defined in differential form by the Langevin equation [26]:

$$dx = \mathbf{A}(x,t)\,dt + \mathbf{B}(x,t)\,dW(t) \tag{22}$$

for a position vector $x(t)$. The matrix $\mathbf{A}$ represents the deterministic background displacement determined by v and, in addition, contains contribution of the dispersion tensor as follows:

$$\mathbf{A}(x,t) = \mathbf{v} + \nabla \cdot \mathbf{D} \tag{23}$$

The displacement matrix $\mathbf{B}$ refers to a stochastic random walk process that incorporates molecular diffusion and dispersion as:

$$\mathbf{B} = \begin{bmatrix} \frac{v_1}{\mathrm{V}}\sqrt{2(\alpha_L \mathrm{V} + D_0)} & -\frac{v_2}{\mathrm{V}}\sqrt{2(\alpha_T \mathrm{V} + D_0)} \\ \frac{v_2}{\mathrm{V}}\sqrt{2(\alpha_L \mathrm{V} + D_0)} & -\frac{v_1}{\mathrm{V}}\sqrt{2(\alpha_T \mathrm{V} + D_0)} \end{bmatrix} \tag{24}$$

The differential $dW(t) = Z\sqrt{\Delta t}$ represents a Wiener process describing Brownian motion in which Δt is time step and Z represent a random number[2].

Consequently, the implementation of the particle tracking model requires a finite difference form of Equation (22) at time step n, which in this model is given by:

$$x_i^n = x_i^{n-1} + A_i \Delta t + \sqrt{\Delta t}\sum_j B_{ij} Z_j \tag{25}$$

In summary, the particle trajectory is computed by a finite difference technique expressed in Equation (25). The first displacement term of this equation $(A_i \Delta t)$ is deterministic, with **A** defined in Equation (23). This expression captures the movement of particles in the streamlines defined by the flow field[3]. The last term in Equation (25), consider the stochastic random walk behavior to simulate dispersion, with the form of the matrix **B** expressed in Equation (24).

So far, it has been taken for granted that the local velocity vector is known at all locations in space. Velocity interpolation within a cell is then determined quickly and easily using the velocity interpolation scheme first derived by Pollock [19]. Using that scheme, the code determines, for a given particle at a given location within the cell, the time required to exit the cell and the location where it leaves. If this time is greater than the time step Δt, the particle location within the cell is computed. If the time is less than the time step Δt, the particle is forced to stop at this location and then proceed in another step within the adjoining cell. This process is repeated until the ending time Δt is reached.

For this method to work properly, the time step must be selected such that, on average, a particle takes several time steps within each cell. In a system with large variations in pore-water velocity due to permeability and porosity differences from cell to cell, the appropriate time step can vary greatly throughout the domain. Here, this factor is accounted for by dynamically determining the characteristic time steps in an approach similar to that developed by Wen and Gomez-Hernandez [21]. In a given cell, the magnitude of the velocity in the cell is used to scale the time step. The time required to traverse the cell completely in each of the three coordinate directions is computed, and the minimum is determined. This approach ensures that several steps are taken by a particle within a cell but minimizes computational time by tailoring the time step to the characteristic velocity within each cell.

The problem examined here is a first contact miscible flood in which a displacing fluid is injected into a porous medium initially saturated with a resident fluid that is miscible in all proportions with the displacing fluid. The procedure of this method in each time step is as follows:

The concentrations of each grid block are updated by counting the number of particles in the given block.

Pressure equation is solved to obtain pressure field.

Velocity field is calculated using Darcy's law and pressure field.

The new particles are generated that representing the amount of displacing fluid injected during the current time step.

The particles are moved to new positions by two different mechanism, convection and dispersion.

New concentrations are calculated.

The viscosity μ_m of the mixed zone is estimated from the following empirical law [22]:

$$\frac{\mu_o}{\mu_m} = \left(CM^{1/4} + 1 - C\right)^4 \tag{26}$$

where C is the solvent concentration, $M = \mu_o/\mu_s$ is the mobility ratio, μ_s and μ_o are the viscosity of the solvent and oil (the displaced fluid), respectively.

3. Results and Discussion

Figure 6 shows detail and scale coefficients of transformed fine map (Figure 5) in two different levels. In the sub figures 6a, 6b and 6c, 0th (fine map), 1st and 2nd decomposition levels using Equations (9) and (10) have been shown respectively.

Figure 7 shows the coarsened (compressed) map generated by inverse wavelet transform with $\tau_S = \tau_D = 0.8$ in two levels. In the sub figures 7a, and 7b, 1st and 2nd compression of the fine map (Figure 5 or Figure 6a) using the mentioned procedure have been shown respectively. In each sub figure, data compression percentage (eliminated data) has been shown. It shows that the wavelet transform is a powerful tool for image compression. The straightforward procedure of image compression using wavelet transformation is its useful property.

Figures 8a, 8b, 8c, and 8d show the corresponding fine and coarsened blocks configurations in different levels, which leads us to fluid flow calculations. Recognition of grid cell network configuration is the other good result of wavelet transformation. Using this good feature one can construct the coarsened grid block configurations (coarse block size and location) to compute the flow problem.

Figure 9 shows the results of single-phase flow problem for fine and two levels of coarse-scales. As can be seen from these figures, the results of single-phase flow problem with **14255** deleted data points (**87%** compression) still show very good agreement with full fine-grid simulation. The maximum RMS error for coarsened map is **0.23**, which is low. It should be mentioned that for full fine-scale problem, we ought to solve **16384** equations whereas, with 2nd level coarsened model we only ought to solve **2129** equations, which reduces the size of the problem with factor **7.7**. Thus an approximate solution is obtained without ever having to solve the full fine-grid problem, saving CPU time and memory.

Figure 10 shows simulation results of the miscible displacement process for fine and 1st level of coarse-scale at two pore volume injected (PVI). The dispersion parameters of this simulation are as follows:

$$\alpha_L = 1.57 \times 10^{-3}\ \mathrm{cm^2/s} \quad , \quad \alpha_T = 4.84 \times 10^{-5}\ \mathrm{cm^2/s}$$

The specific boundary conditions are Dirichlet type (constant pressure) in direction of flow and Neumann type (no-flow or impermeable) in perpendicular direction of

flow. Also, the result shows the reasonable agreement between full fine and coarse-scale problem.

4. CONCLUSIONS

Here, we proposed a novel upscaling method based on wavelet transformations, which is applicable to wide variety of heterogeneous media. The method generates a highly efficient grid structure (in terms of the number of the blocks in the coarsened model), and is computationally highly efficient, because it uses irregular but still Cartesian grid can reduce drastically the number of grid blocks, and hence the number of equations to be solved. Moreover, since the effective properties of the coarsened blocks are computed automatically, it is very cost efficient, whereas, in the most efficient upscaling methods currently available, the effective properties of the coarsened blocks are estimated by carrying out single phase flow calculations which particularly in 3D are highly costly.

One of the most important aspects of any upscaling methods, in addition to its accuracy, is the ease and efficiency by which the method can be implemented. This is particularly important, as one has to deal with a large grid that must be successfully and efficiently upscaled. Here, we point out two crucial points to demonstrate the efficiency of proposed method. (1) Calculation of wavelet coefficients is done by completely localized operations, the ideal condition for parallel computations. It is a very useful virtue if a very large fine-grid model represents the original geological model. None of the previous upscaling methods are easily parallelizable, if at all. (2) With a fine-scale mesh of n blocks, the computation time in the most efficient upscaling methods currently available is either order of n^2 [18], or is order of n^3 [9], whereas, as is well known in the theory of wavelets, it is only $n \log n$ for calculation of the wavelet coefficients, which is the most time consuming part of the proposed method. Thus, the computation time of the proposed method is order of magnitude less than that of the most efficient and accurate previous methods.

5. SUBSCRIPTS

[1] The filter coefficients are related to each other by:

$$g_n = (-1)^n h_{L-n-1} \quad , \quad n = 0,1,\ldots,L-1$$

where $L = 2M$ (compactly supported wavelets of order M have the zero first M moments). For Haar wavelets $M = 1$.

[2] Z is selected from a uniform distribution for example Gaussian.

[3] The term $\nabla \cdot \mathbf{D}\Delta t$ is required to correctly reproduce the transport equation for cases in which there are gradients in velocity or dispersion coefficient. It reduces to zero for uniform flow fields and constant dispersivity. What is retained in this case is transport along the flow streamline governed by the flow field

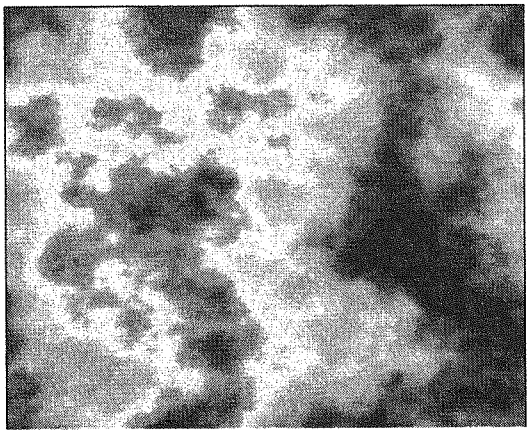

Figure 6a- Fine permeability map fBm 128×128 with H=0.8

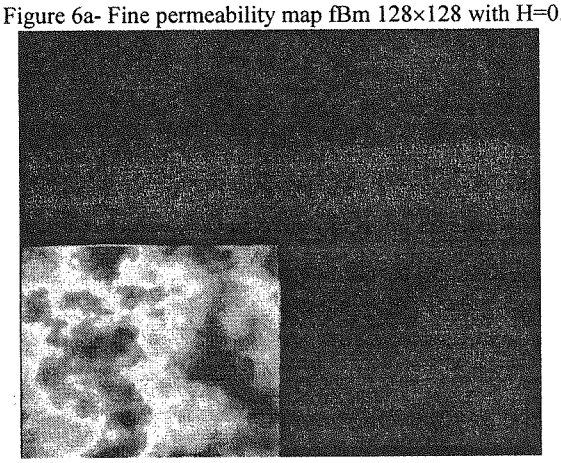

Figure 6b- 1st level decomposition

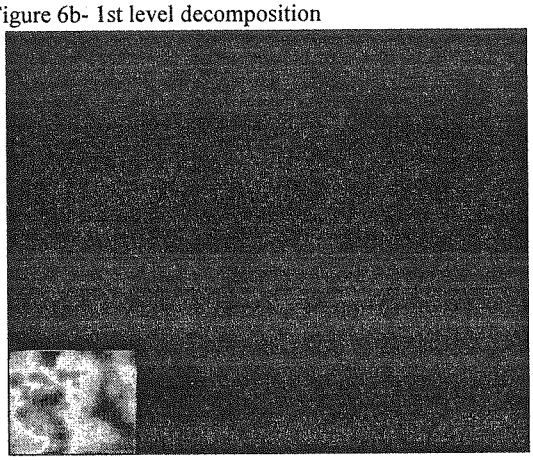

Figure 6c- 2nd level decomposition

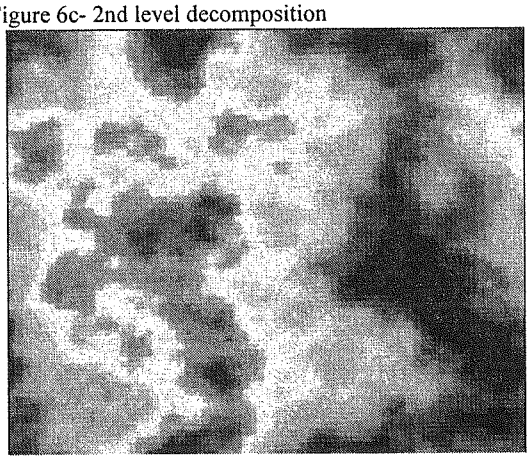

Figure 7a- 1st level compression (70 %coarsened)